Velocity analysis of migrated seismic data after structural interpretation

Jos van Trier

ABSTRACT

Residual velocity analysis is often still necessary after the determination of a global structural-velocity model. Reflection events in the unstacked migrated data can be used for this analysis. The depth variations of these events are inverted to find local velocity perturbations, where the variations are either determined from picking the events, or from semblance calculations.

INTRODUCTION

In an article in the previous SEP report (Van Trier, 1988) I described a method to refine the result of a structural-velocity optimization. Residual variations in the depth of reflectors in the migrated data are picked and converted to traveltime perturbations, and a tomographic matrix calculated in the initial velocity analysis is used to find local velocity perturbations.

In this paper I review the main points of the theory presented in the previous one, and I present a small synthetic-data example to verify assumptions I have made in the derivation of that theory. Furthermore, I extend the method to use a semblance norm instead of picked events, making it more robust in the presence of noise. Finally, I discuss some of the problems that arise when the reflectors are not accurately known.

THE DATA SPACE: A SIMPLE EXAMPLE

In this section I present a synthetic data example merely to make the reader familiar with the migrated-data space. The example has little relevance in the real world, but shows how a small anomaly in the velocity model shows up in the migrated data.

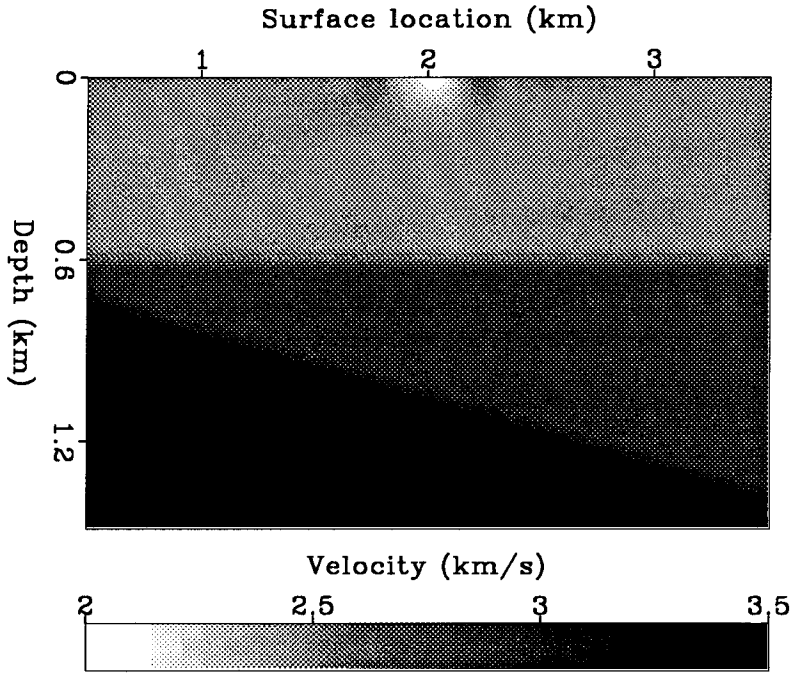

FIG. 1. Velocity model with anomaly at the surface. The velocity in the center of the anomaly is 2 km/s, the velocity in the top layer 2.5 km/s.

Synthetic shot profiles are generated for a velocity model that contains a flat and dipping reflector and a small anomaly near the surface (Figure 1). The velocity in the center of the anomaly is 20 % smaller than the surrounding velocity. Figure 2 shows an example of a synthetic shot profile. The profiles are migrated with a velocity model without the anomaly. Figure 3 shows the migration of the profile in Figure 2, Figure 4 shows a slice through the migrated data at a constant surface location (CSL) of 1.8 km, and Figure 5 shows a depth slice at a depth of .624 km. Each of these three panels shows the effect of the anomaly on the migration result; the effect is most distinct in the depth slice, and the pattern of the perturbation is the representation of Kjartansson's "vees" (Kjartansson, 1979; Woodward, 1987) in migrated space. Figure 6 shows the final stacked migrated image. The depth perturbations due to the velocity anomaly are canceled when stacked together, and the image gives an accurate representation of the position of the reflectors in the model.

INVERSION USING PICKED EVENTS

In SEP-57 (Van Trier, 1988) I propose to pick events on the CSL gathers and to invert them to find local velocity perturbations. I make two assumptions in the inversion: first, that events can be picked accurately in the migrated data, and second, that the velocity model is known well enough to pick the reflector positions more or less correctly from the stacked migrated image. In the next sections I

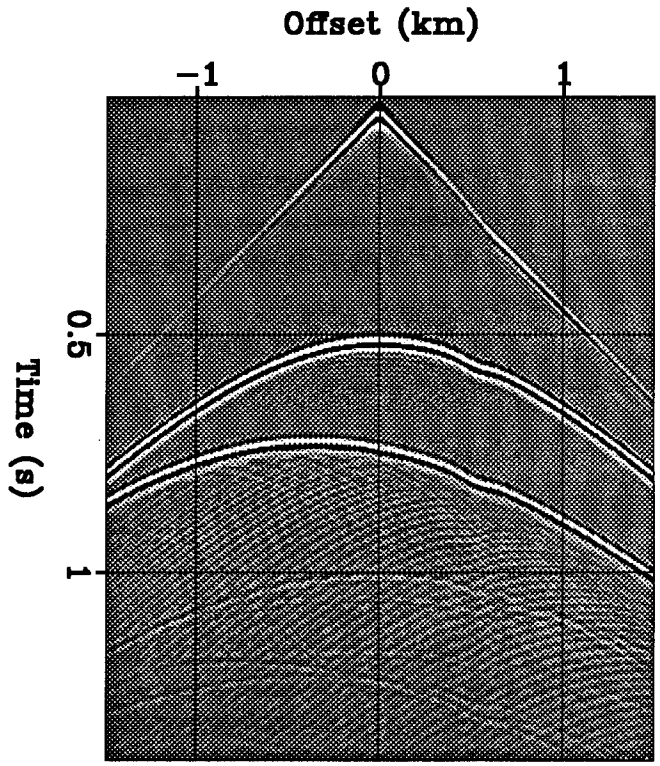

FIG. 2. Shot profile with shot located at 1.5 km.

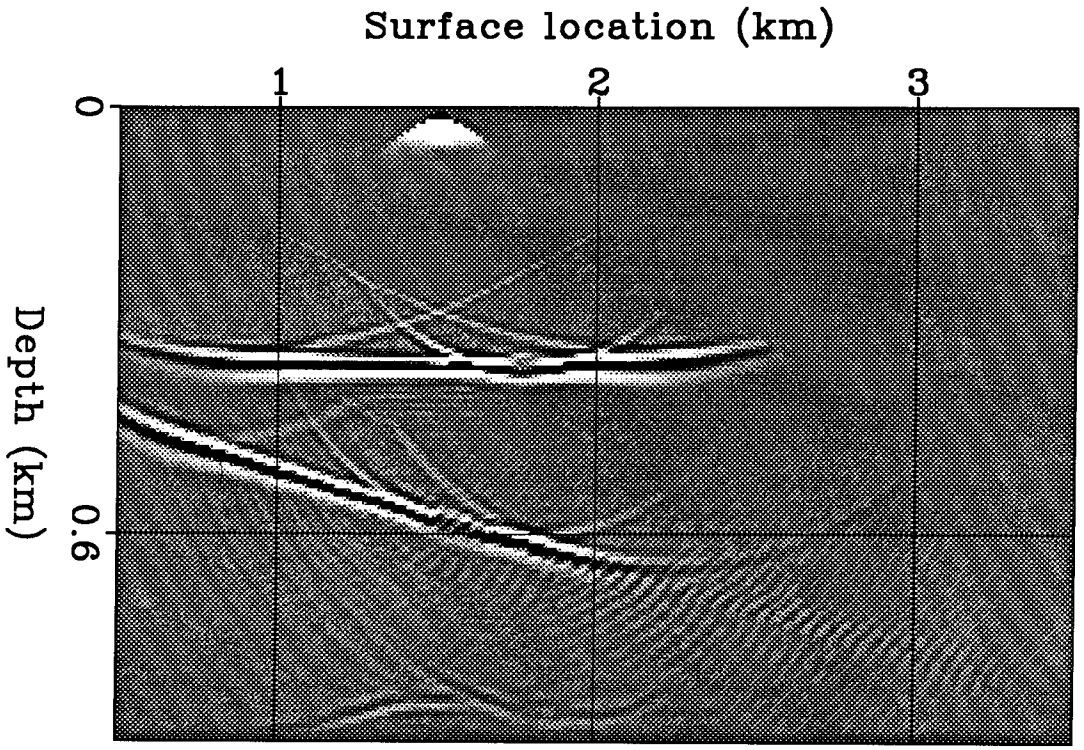

FIG. 3. Migrated shot profile of shot located at 1.5 km.

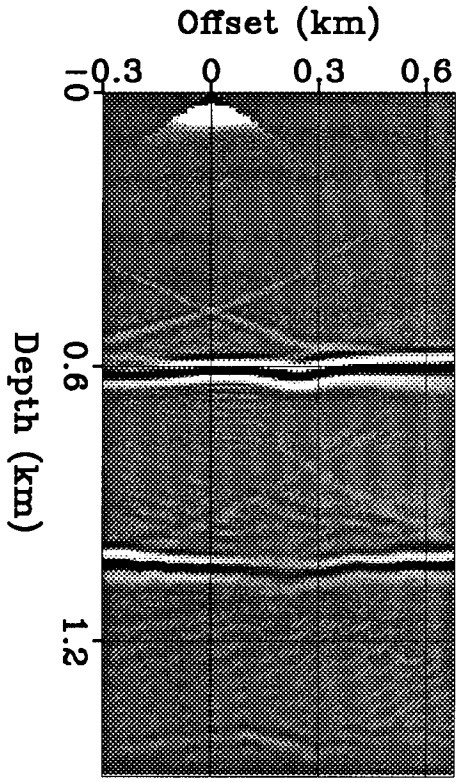

FIG. 4. CSL gather at surface location of 1.8 km.

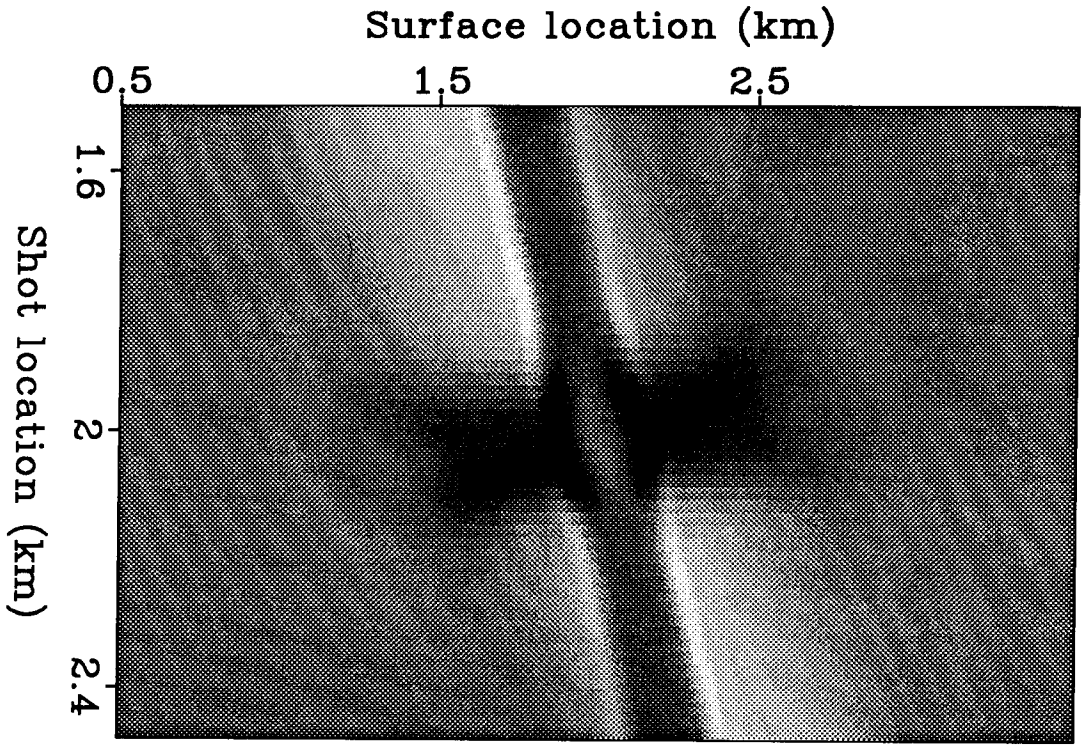

FIG. 5. Depth slice through migrated data at a depth of .624 km.

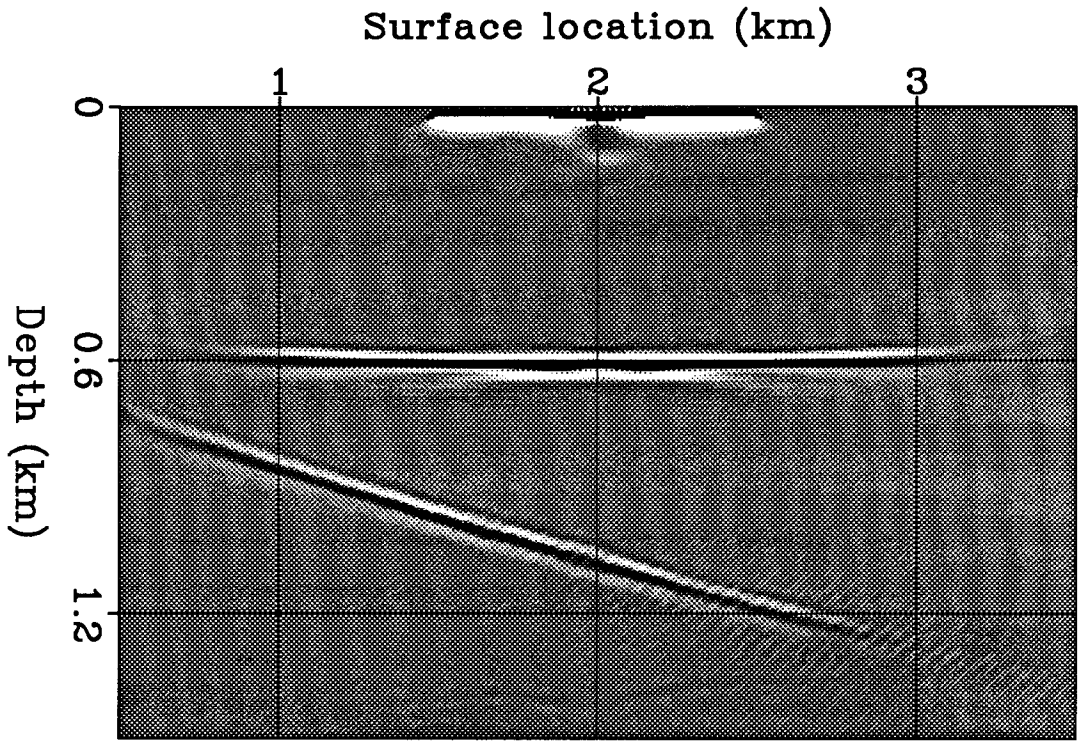

FIG. 6. Stacked migrated image.

describe how to extend the method beyond each of these limitations, but first I review the main points of the method presented in SEP-57.

For easy reference I have reproduced Figure 1 of SEP-57 here as Figure 7. Assuming that reflectors can be picked from the migrated image, rays can be traced upwards from the reflectors to the surface, and a tomographic matrix can be constructed that linearly relates traveltimes of the rays with model parameters, $\mathbf{p}$:

$$\begin{pmatrix} \mathbf{A}_{-\theta} \\ \mathbf{A}_{+\theta} \end{pmatrix} \mathbf{p} = \begin{pmatrix} \mathbf{t}_{-\theta} \\ \mathbf{t}_{+\theta} \end{pmatrix}, \tag{1}$$

where $\mathbf{t}_{-\theta}$ is the vector containing the traveltimes to the sources, and $\mathbf{t}_{+\theta}$ the vector containing the traveltimes to the receivers. $\mathbf{A}_{-\theta}$ and $\mathbf{A}_{+\theta}$ are the matrices that model these respective traveltimes from the model parameters. The matrices $\mathbf{A}$ are calculated by raytracing. A new matrix is constructed by summing $\mathbf{A}_{-\theta}$ and $\mathbf{A}_{+\theta}$:

$$\mathbf{B} = \mathbf{A}_{-\theta} + \mathbf{A}_{+\theta}. \tag{2}$$

This matrix models traveltimes from sources to receivers for selected depth points as a function of reflection angle:

$$\mathbf{B}\,\mathbf{p} = \mathbf{t}_{-\theta} + \mathbf{t}_{+\theta} = \mathbf{t}_{\mathbf{h}}, \tag{3}$$

with $\mathbf{t}_h$ the traveltimes as a function of the offset h in the CSL gather.

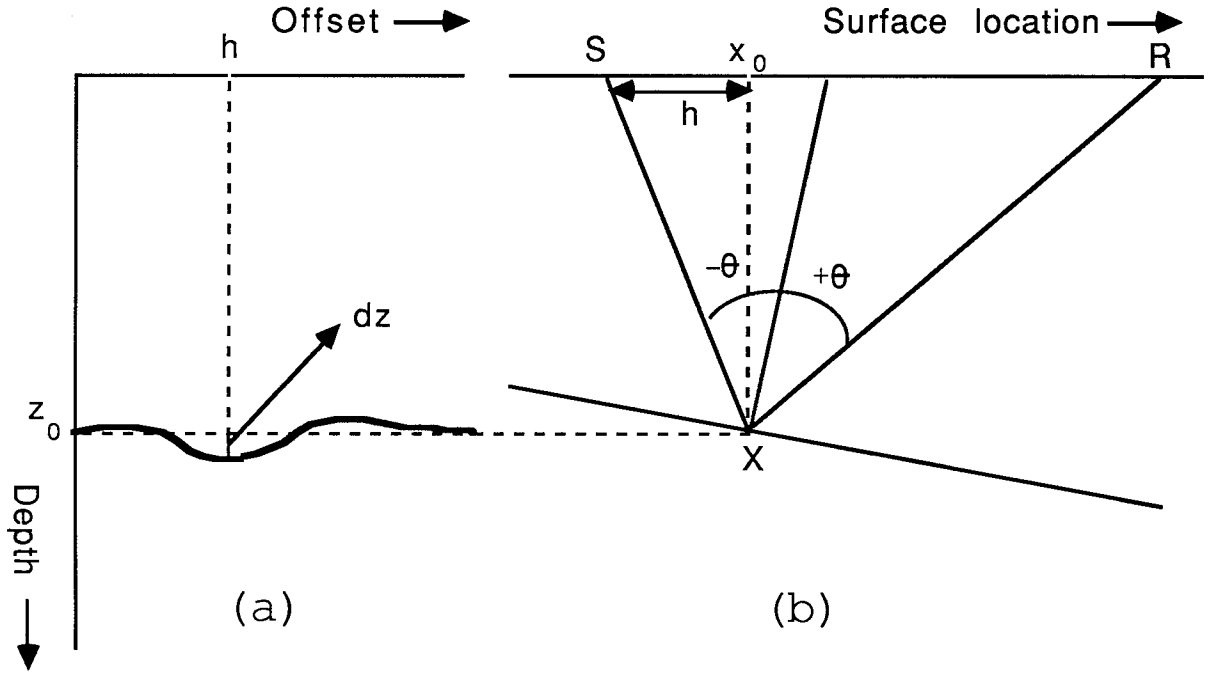

FIG. 7. CSL gather after migration with the structural model (a), and corresponding ray picture (b). The small variations δz in the event are caused by local velocity anomalies.

Ignoring any wave effects, a spike at (h, x_0, z_0) in the CSL gather at surface location x_0, can be found in the original seismic data at

$$(s, g, t_{SX} + t_{XR}) = (s, g, t_{-\theta} + t_{+\theta}), \tag{4}$$

with s the source position, g the geophone position, t_{SX} the traveltime of the ray traveling from S to X, and t_{XR} the traveltime of the ray traveling from X to R. The position of the source S is related to the offset in the CSL ($h = x_0 - s$), the position of the receiver R has to be determined from ray tracing (see figure 7).

An average velocity for the point (h, x_0, z_0) in the CSL gather can now be defined as:

$$\overline{v}(h, x_0, z_0) = \frac{s_{-\theta} + s_{+\theta}}{t_{-\theta} + t_{+\theta}}, \tag{5}$$

where $s_{-\theta}$ is the length of the ray traveling from source to reflector, and $s_{+\theta}$ the length of the ray traveling from reflector to receiver. Both the traveltimes and the ray lengths in equation (5) are known from ray tracing.

Consider an event in the CSL gather at depth z_0. Perturbations δz in the depth of the event as a function of offset can be converted to traveltime perturbations δt using the average velocity $\overline{v}$:

$$\delta t(h, x_0, z_0) = \frac{\delta z(h, x_0, z_0)}{\overline{v}(h, x_0, z_0)} \tag{6}$$

Here I have assumed that the reflection point of the perturbed data point is (x_0, z_0), that there is no lateral movement of the picked data point, and that the velocity anomaly is only reflected in the traveltime (see also one of the next sections).

As in standard tomography problems, the matrix **B** can now be used to relate the traveltime perturbations to velocity perturbations, $\delta\mathbf{p}$:

$$\delta\mathbf{t}_h = \mathbf{B}\delta\mathbf{p}. \tag{7}$$

The velocity perturbations are found by inverting the matrix using standard techniques.

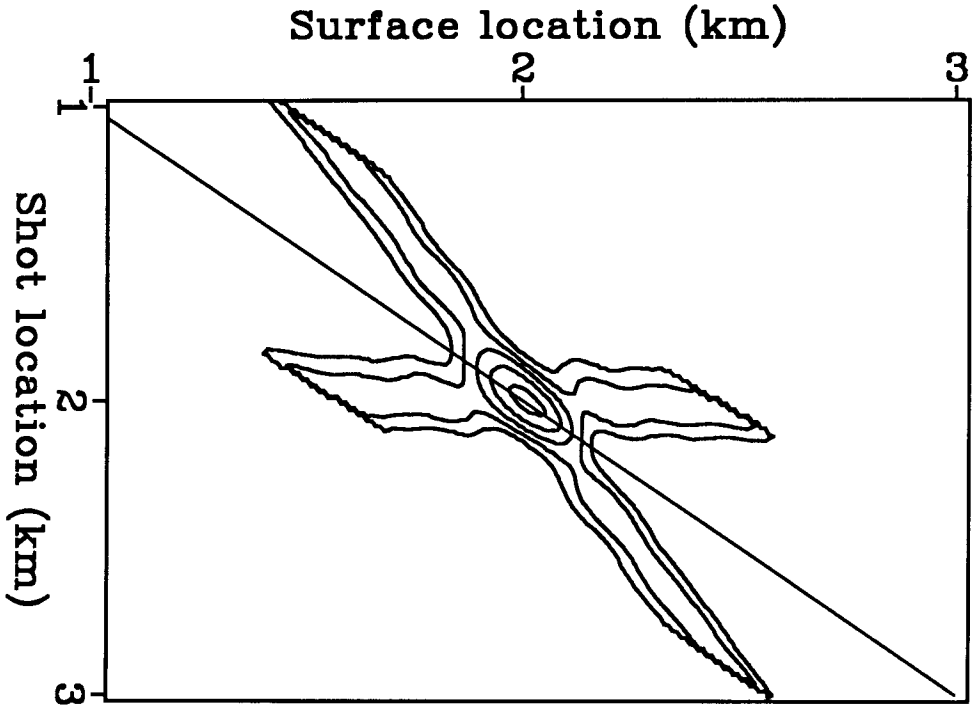

FIG. 8. Ray-theoretic depth anomalies calculated for the velocity model of Figure 1. Contours are plotted at 5 m intervals; the depth perturbation in the center of the vees is 25 m. The diagonal line represents zero offset.

Equation (5) can be used to construct ray-theoretic depth anomalies for the example I have shown before: the difference in traveltimes of rays traced through the reference model and rays traced through the model with the anomaly are converted to depth anomalies. The result is shown in Figure 8. The cutoffs in the anomalies are caused by the finite cable length. Figure 9 shows the same figure overlaid on Figure 5. The patterns of the wave-theoretic and ray-theoretic anomalies have about the same shape and amplitude, meaning that, at least for this rather superficial example, equation (5) can be used to convert depth anomalies to traveltime anomalies, which can then be inverted. Another assumption, the one that the migrated image is accurate enough to pick reflectors, is also valid, as is shown in Figure 6.

However, already in this simple example, it can be seen that the perturbations are much more ill-defined in the wave-theoretic case than in the ray-theoretic case,

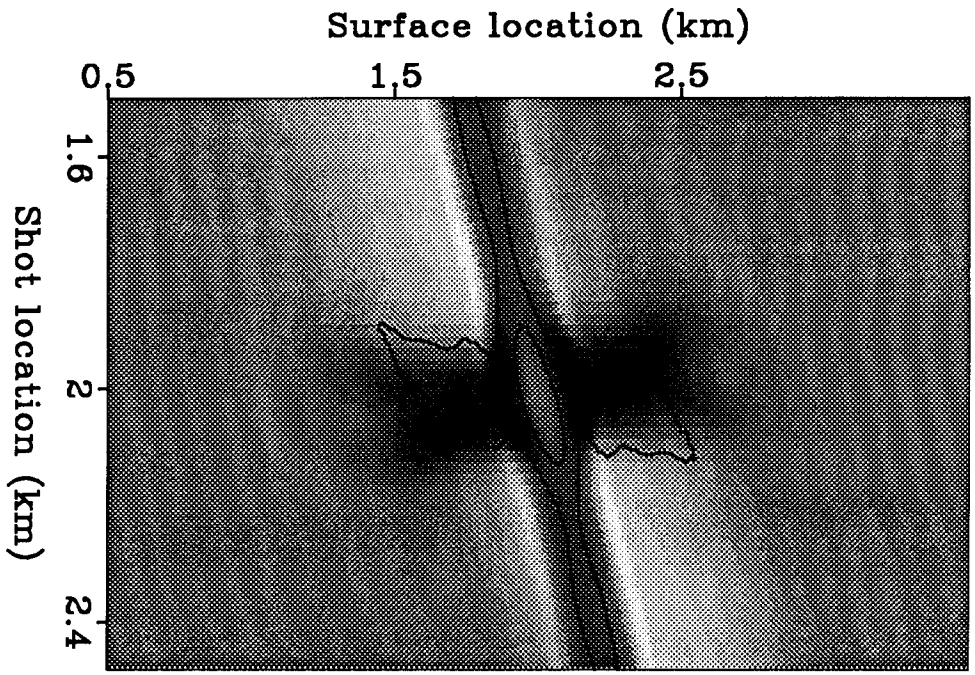

FIG. 9. Ray-theoretic depth anomalies of Figure 8 plotted on top of Figure 5. The contour lines denote 10 and 20 m depth anomalies, respectively. The depth slice is taken at 624 m depth. Ray theory predicts only the center perturbation; the length of the wavelet causes the distinct pattern.

because of the limited bandwidth of the source. In the presence of noise this problem will only get worse, and it remains to be seen if the inversion will give a meaningful result. Furthermore, the anomaly in the perturbed model is sufficiently small to give an accurate image when all migrated profiles are stacked together. Larger anomalies will give a less accurate image. I will address the latter problem in the last section, but first I discuss how to deal with the noise problem.

SEMBLANCE CRITERION

Instead of using picked depth perturbations, the semblance of the stacked image can be used in the velocity determination. A semblance criterion can not overcome the limited bandwidth of the source, but can make the inversion more robust with respect to noise. The total semblance can be defined as:

$$S(x,z) = \sum_x \sum_z \frac{1}{2} \frac{\left(\sum_h d(x,z,h)\right)^2}{\sum_h d^2(x,z,h)} = \sum_x \sum_z \frac{1}{2} \frac{I_1^2}{I_2}, \tag{8}$$

with $d(x,z,h)$ the migrated data at (x,z,h). To average out wave effects, S is often combined for different depth levels using a moving average window of about the length of the seismic wavelet. The summation over z formally extends over the complete depth range of the migrated data. However, since the migrated image is

reasonably well-determined at this stage, the summation can be limited to certain windows centered around the locations of the reflectors in the migrated image. In the rest of the equations, I keep the summation over z for convenience.

Derivatives of the semblance with respect to the model can be written as:

$$\frac{\partial S}{\partial \mathbf{p}} = \sum_x \sum_z \frac{I_1 I_2 - I_1^3}{I_2^2} \sum_h \frac{\partial d}{\partial \mathbf{p}}(x,z,h). \tag{9}$$

The last sum in the right-hand expression can be written in terms of x, z and h using the chain rule:

$$\sum_h \frac{\partial d}{\partial \mathbf{p}} = \sum_h \Big(\frac{\partial d}{\partial x}\frac{\partial x}{\partial \mathbf{p}} + \frac{\partial d}{\partial z}\frac{\partial z}{\partial \mathbf{p}} + \frac{\partial d}{\partial h}\frac{\partial h}{\partial \mathbf{p}}\Big). \tag{10}$$

Assuming that the reflector point moves perpendicular to the reflector, the movement of the reflector can be related to the change in arclength:

$$\begin{aligned} \delta x &= \delta s \, \sin(\phi); \\ \delta z &= \delta s \, \cos(\phi), \end{aligned} \tag{11}$$

with ϕ the dip at the reflector. Equation (10) can now be written in terms of traveltime using the above equation and the relation $s = \overline{v}t$ (a generalization of equation (5)):

$$\sum_h \frac{\partial d}{\partial \mathbf{p}} = \sum_h \Big(\frac{\partial d}{\partial x}\,\overline{v}\sin(\phi)\frac{\partial t}{\partial \mathbf{p}} + \frac{\partial d}{\partial z}\,\overline{v}\cos(\phi)\frac{\partial t}{\partial \mathbf{p}} \Big). \tag{12}$$

In the above expression, lateral changes in the data point have been ignored ($\frac{\partial h}{\partial \mathbf{p}} = 0$), as was done in equation (5). Substituting this expression in equation (9), the expression for the gradient vector $\mathbf{g}$ of the semblance with respect to the model parameters becomes:

$$\mathbf{g} = \mathbf{B}^T\mathbf{q}. \tag{13}$$

Here $\mathbf{B}$ is the same matrix as in equation (7), and $\mathbf{q}$ is a vector that is calculated from the migrated data. Expressions for the elements of $\mathbf{g}$ and $\mathbf{q}$ are:

$$g_i = \frac{\partial \mathrm{S}}{\partial \mathrm{p_i}}, \quad \mathrm{i} = 1,\mathrm{N}; \tag{14}$$

$$q_j = \frac{\mathrm{I_1 I_2 - I_1^3}}{\mathrm{I_2^2}}\Big(\overline{\mathrm{v}}\sin(\phi)\frac{\partial \mathrm{d_j}}{\partial \mathrm{x}} + \overline{\mathrm{v}}\cos(\phi)\frac{\partial \mathrm{d_j}}{\partial \mathrm{z}} \Big), \quad \mathrm{j} = 1,\mathrm{M}, \tag{15}$$

with N the number of parameters, and M the number of data observations (the index j denotes a data point (x,z,h)). For field data, the derivatives with respect to x and z have to be determined in a robust way, for example by taking derivatives of the smoothed envelope of the data, rather than of the data signal itself.

Equation (13) provides an expression for the model gradient vector that can be used in an iterative optimization scheme, such as conjugate gradients. At each step

in the optimization, the semblance needs to be evaluated several times when the model space is searched for the optimal model. If the semblance would be calculated after remigrating the data, these searches could become prohibitively expensive. However, since depth perturbations can be approximately forward modeled using equations (7) and (5), such remigrations are not necessary: instead, the semblance is calculated by summing the data over perturbed depth curves.

REMARKS

In the previous section, I have shown a method that avoids picking of the migrated data. I have not yet discussed the other problem: the limited accuracy of the migrated image. In the above approaches I have assumed that the migrated image is accurate enough to pick reflectors. Then Fermat's principle can then be used: in first order approximation raypath variations can be ignored and only traveltime perturbations have to be considered. Furthermore, I have used an approximate expression for converting depth perturbations to time perturbations (equation (5), and the expression used in equation (12), which is somewhat more general). In reality, not only the reflector point, but also the data point moves when the velocity model is perturbed. In other words, the inversion problem is more complicated than a standard tomographic problem, because an additional transformation of the data (the migration) has taken place, where the transformation depends on the velocity model, and the model is just the unknown that needs to be determined. Therefore, it remains to be seen if Fermat's principle is applicable to this problem. I am currently working on some extensions to the inversion that make less assumptions on the movement (or rather fixation) of the reflector.

CONCLUSIONS

I have presented two different approaches to the inversion of migrated data with picked boundaries: one using picked traveltimes of reflection events in the data, and another using a semblance norm. The first approach might provide a better resolution when the events are well-defined, the second provides a more robust scheme in the case of noisy data.

REFERENCES

Kjartansson, 1979, Attenuation of seismic waves in rocks: Ph.D. thesis, Stanford University.

Van Trier, J., 1988, High-resolution velocity inversion of migrated data after structural interpretation: SEP–**57**, 139-144.

Woodward, M., 1987, Reflection tomography: vees in midpoint-offset space: SEP–**51**, 1-12.